HHS Public Access

Author manuscript

Abdom Imaging. Author manuscript; available in PMC 2017 August 02.

Published in final edited form as:

Abdom Imaging. 2015 March ; 40(3): 578–586. doi:10.1007/s00261-014-0246-2.

Comparison of calculated and acquired high b-value diffusion weighted imaging in prostate cancer

Kinzya B. Grant, M.D.[1], **Harsh K. Agarwal, Ph.D.**[1,2], **Joanna H. Shih, Ph.D.**[3], **Marcelino Bernardo, B.S.**[1,4], **Yuxi Pang, Ph.D.**[5], **Dagane Daar, R.T.**[1,4], **Maria J. Merino, M.D.**[6], **Bradford J. Wood, M.D.**[7], **Peter A. Pinto, M.D.**[8], **Peter L. Choyke, M.D.**[1], and **Baris Turkbey, M.D.**[1]

[1]Molecular Imaging Program, NCI, NIH, Bethesda, MD, USA

[2]Philips Research North America, Briarcliff Manor NY, USA

[3]Biometric Research Branch, Division of Cancer Treatment and Diagnosis, NCI, NIH, Bethesda, MD, USA

[4]Leidos Biomedical Research, Inc., Frederick National Laboratory for Cancer Research, MD, USA

[5]Philips Healthcare, Cleveland, OH, USA

[6]Laboratory of Pathology, NCI, NIH, Bethesda, MD, USA

[7]Center for Interventional Oncology, NCI and Radiology and Imaging Sciences, Clinical Center, NIH, Bethesda, MD, USA

[8]Urologic Oncology Branch, NCI, NIH, Bethesda, MD, USA

Abstract

Purpose—To determine whether the performance of calculated high b-value diffusion weighted images (DWI) derived from regular lower b-value DWI using exponential diffusion decay models (intravoxel incoherent motion=IVIM and diffusional kurtosis=DK) is comparable to acquired high b-value DWI in prostate cancer detection.

Materials and Methods—One hundred six patients underwent diagnostic multiparametric prostate MRI at 3T using an endorectal coil. 5 b-value (b= 0, 188, 375, 563, 750 s/mm^2) DWI and high b-value (b=0, 1000 and 2000 s/mm^2) DWI were acquired. Calculated high b-value (b=1000 s/mm^2 and b=2000 s/mm^2) DWI were derived from the DWI dataset using DK and IVIM models. Calculated and acquired high b-value DWI images were compared for lesion visibility and image quality by two experienced radiologists (1 and 6 years of experience). GEE with Wald test was used to compare the image quality among the four calculated high b-value DWI by comparing the proportion of lesions in each model which were comparable to the acquired images. This comparison was done for all lesions and by lesion location (PZ or CG; low apical/anterior or apical/mid/base).

Results—More lesions were visible on acquired b=2000s/mm^2 compared to b=1000s/mm^2 DWI. Calculated high b value DWI using the IVIM model had approximately the same number of

Address correspondence to: Baris Turkbey M.D., Molecular Imaging Program, National Cancer Institute, 10 Center Dr, MSC 1182, Bldg 10, Room B3B85, Bethesda, MD 20892-1088, turkbeyi@mail.nih.gov.

lesions as acquired high b value DWI whereas the DK model had fewer lesions than acquired images. The image quality of calculated high b value DWI was comparable to that of acquired images and the highest quality images were obtained with $b1000_{IVIM}$. The image quality of calculated $b1000_{IVIM}$ was the same as that of acquired DWI in apical/mid/base (98%) locations and comparable in low apical & anterior (95.4%) locations. The image quality of calculated $b2000_{IVIM}$ was inferior in both apical/mid/base (86.2%) locations and comparable in low apical & anterior (83.9%) locations.

Conclusion—Calculated high b-value DWI obtained using IVIM model has same lesion visibility as that of acquired DWI. The image quality of calculated high b value DWI relative to corresponding acquired DWI decreases with increase in b-value.

Keywords

prostate cancer; MRI; Diffusion-weighted imaging; high b value

Introduction

Multiparametric MR imaging (mpMRI) has become the imaging method of choice for local detection and staging of prostate cancer [1,28]. Although reported sensitivities and specificities of mpMRI for the detection of prostate cancer vary widely in the current literature, prostate mpMRI is emerging as a valuable imaging tool in localizing suspicious lesions for targeted biopsy, and has potential to replace the random prostate biopsy with TRUS-MRI fusion guided biopsy [2,33]. Among the most important and reliable components of an mpMRI is diffusion weighted imaging (DWI). DWI reflects the amount of Brownian motion of water molecules within tissues by means of diffusion sensitizing gradients (b-values). Restricted water diffusion, as is seen in most tumors due to high cellular density, results in limited mean water path lengths during scan acquisition resulting in low signal on quantitative apparent diffusion coefficient (ADC) maps obtained using the classical Stejskal-Tanner diffusion decay model [3–5]. In the case of prostate cancer, ADC values correlate with tumor aggressiveness as determined by the Gleason score of the tumor; lower ADC values are associated with higher Gleason scores both at 1.5T and 3T [6–10]. These studies have employed DWI acquired with a range of b-values less than b=1000 s/mm^2 not only because the classical Stejskal-Tanner diffusion decay model fails at higher b-values [11–14] but also due to inadequate signal to noise ratio (SNR) above b=1000 s/mm^2 DW images [15].

Recently, the value of high b-value (b>1000 s/mm^2) DWI has been recognized for prostate cancer [16–24]. At higher b values, tissue with high mean water molecule path lengths (i.e. normal tissue) tends to lose signal rapidly while tissues with restricted water diffusion yield relatively higher signal. However, these images typically suffer from low signal to noise ratios and may be difficult to interpret. Qualitative analysis of DWI obtained at b = 1000 s/mm^2 and b = 2000 s/mm^2 suggest that high b-value DWI improves sensitivity of MR for high-grade prostate cancers [24]. An alternative, however, to acquiring high b-value DWI is to calculate them from DWI acquired as part of prostate mpMRI using one of several available extrapolation models. Thus, it may be possible to achieve the benefits of high b-value images without actually acquiring them, both saving time and improving image quality

due to higher SNR [25]. It is unclear, however, whether calculated high b value DWI is diagnostically equivalent to acquired high b-value DWI. In this study, we aim to directly compare the performance of acquired and calculated DWI for the detection of prostate cancer at b-values of 1000 and 2000 s/mm^2 using two different models for calculation, the intravoxel incoherent motion (IVIM) and the diffusional kurtosis (DK) models.

Materials And Methods

Study Design and Population

This retrospective, single-institution study was approved by the local institutional review board. The study was compliant with the Health Insurance Portability and Accountability Act and informed consent was obtained from each patient. During an 8 month period (01/12/2012 to 09/12/2012), 350 consecutive patients underwent mpMRI of the prostate. Indications for prostate mpMRI were prostate cancer detection in patients with elevated serum PSA with or without prior random transrectal ultrasound (TRUS) biopsy, and local staging for previously diagnosed cancer. Inclusion criteria were (a) having an mpMRI of the prostate, which also included acquisition of high b-value DWI, and (b) subsequent MR/TRUS fusion guided prostate biopsy of the lesions identified on mpMRI. 170 patients were excluded since they did not have MR/TRUS fusion guided biopsy. Additionally, 60 patients were excluded because high b-value DWI was not obtained. Reasons for not acquiring the high b-value DWI were often related to limited examination time secondary to claustrophobia. Finally, fourteen patients were excluded due to artifacts (e.g. hip replacements). The final study population consisted of 106 patients. The study population flow chart is presented in Figure 1. The median age of the included patients was 65 years (mean: 64 years, range: 43–78 years). The median serum PSA value was 5.35 ng/mL (mean: 7.9 ng/mL, range: 0.5–51 ng/mL). The average time to MR/TRUS fusion guided biopsy following prostate mpMRI was 28 days (range: 1–109 days, median: 23 days, mode: 1 day).

Multi-parametric MR Imaging

MpMRI of the prostate was performed on a 3T MR scanner (Achieva-TX, Philips Healthcare; Best, NL) using the anterior half of a 32-channel SENSE cardiac coil (Invivo; Gainesville FL, USA) and an endorectal coil (BPX-30, Medrad; Indianola PA, USA). No pre-examination bowel preparation was required. The balloon of each endorectal coil was distended with approximately 45 mL of perfluorocarbon (Fluorinert FC-770, 3M; St Paul MN, USA) to reduce imaging artifacts related to air-induced susceptibility.

MpMRI of prostate consisted of high resolution T2 weighted (T2W) images in 3 orthogonal planes, axial DWI, axial high b-value DWI, MR spectroscopic images and dynamic contrast enhanced MR images. Parameters for the DWI acquired at our center as part of the mpMRI (referred to as regular b-value DWI) and high b-value DWI (referred to as *acquired high b-value DWI*) sequences are presented in Table 1. Imaging parameters of the two DW MRI sequences were chosen to have the same echo times to avoid any bias arising from probing different compartments of diffusion with different T2 values. The acquisition times to generate a regular b-value DWI and high b value DWI vs. regular b-value DWI with

calculated high b-value DWI at b=1000 and 2000s/mm^2 images were 8 min 31 sec vs. 4 min 47 sec (Table 1).

MR/TRUS Fusion Guided Biopsy and Histopathological Analysis

Targeted biopsy of suspicious lesions detected on mpMRI was performed using an MR/TRUS fusion biopsy system [26]. Suspicious lesions were identified on mpMRI by two radiologists (BT and PLC, with cumulative experience of 6, 10 years for prostate MRI) as part of the clinical practice at our institution (It should be noted that acquired high b-value DWI was not used in the radiologists` reading.). In the biopsy suite, a 3D ultrasound (TRUS) was obtained and the prostate was segmented. The segmented MRI and TRUS images were fused volumetrically and the targeted suspicious lesions were transferred from MRI to US so that they became visible as virtual targets on TRUS. Two needle biopsies were obtained from each lesion using two orthogonal planes. This system has been previously shown to have an accuracy of 3–4 mm [27].

All biopsy specimens were reviewed by an experienced pathologist (MJM with experience of over 25 years) blinded to MRI findings.

Image Analysis

Calculated high b-value DWI—Calculation of high b-value DWI at b = 1000 and b = 2000 s/mm^2 was performed using 2 different diffusion decay models: IVIM and DK to extrapolate high b-value DWI from regular b- value DWI. Matlab (The MathWorks Inc., Natick, MA) was used for the computation of calculated high b-value DWI. Since the smallest non-zero b-value in the regular b-value DWI dataset is 188 s/mm^2, multi-exponential decay models were further simplified utilizing the assumption that the contribution due to pseudo diffusion would be absent at non-zero b-values [4]. The DK model is shown in Eq. 1, where f represents perfusion fraction, D represents ADC, b represents DW factor and K represents the non-Gaussian contribution of diffusional kurtosis [3–5].

$$\ln(\mathrm{S}(b)/\mathrm{S}_0)=\ln(1-\mathrm{f})-bD+b^2D^2K/6; \qquad (\mathrm{b}>0) \quad [1]$$

When K is set to zero, Eq. 1 becomes the IVIM model.

For the DK model, the perfusion (ln(1–f)), diffusion (D) and kurtosis (K) components and for IVIM model only perfusion and diffusion components were estimated by fitting the 4 non-zero b-values of the regular b-value DWI dataset to the resultant linear equation. The calculated high b-value DW MRI was then computed by extending this linear equation to the corresponding b- values using the estimated perfusion and diffusion components.

Qualitative image analysis—MIPAV (Medical Image Processing, Analysis, and Visualization; National Institutes of Health, Bethesda MD, USA) software was used to qualitatively compare the acquired and calculated high b-value DWI datasets. Acquired and calculated b=1000 s/mm^2 and b=2000 s/mm^2 images, based on IVIM ($b1000_{IVIM}$, $b2000_{IVIM}$) and DK ($b1000_{DK}$, $b2000_{DK}$), were compared. In each session, window levels

were set to be equivalent for visual analysis at b=0 s/mm^2. Double reader (KBG, BT) comparisons were then made between the acquired, calculated IVIM, and calculated DK DWI sets in consensus. To avoid any possible bias from the initial mpMRI, acquired and calculated DW MRI were evaluated at least 12 months post initial mpMRI and were blinded to the mpMRI except the axial T2W MRI which was marked with the targeted lesions. Lesion visibility and image quality were assessed for each lesion on each DWI dataset. The visibility of each lesion was compared on all 6 DWI datasets using a 0 and 1 score corresponding to invisible and visible, respectively. Lesion visibility analysis was performed separately for tumors with maximum dimension less than 10mm and greater than or equal to 10mm on axial MR images. The quality of the images were scored as 0, 1 and 2 corresponding to non-diagnostic, diagnostic but of a lesser quality than the acquired, and comparable in quality to the acquired image, respectively. All MRI analyses were performed blinded to clinical and histopathologic findings.

Statistical Analysis

Simple ratios of target lesions visible on acquired and calculated high b-value DWI were recorded (% visualized= lesions visualized on high b-value DWI/lesions targeted). Similar comparisons were made for tumor positive targets (Gleason 6–9), and low (Gleason 6–7) and high (Gleason 8–9) grade tumor positive targets.

Image quality was assessed at each b-value ($b1000_{DK}$, $b1000_{IVIM}$, $b2000_{DK}$ and $b2000_{IVIM}$) and comparison was made to the acquired b1000 and b2000 images. Formally, generalized estimating equations (GEE) with a logit link function and working independence correlation structure was used to estimate the proportion of lesions in each model which were comparable to the acquired imaging (i.e., the proportion of lesions with score 2) and the Wald test was used to test the difference in the proportions between these models. This analysis was repeated for TZ and PZ, as well as each region of the prostate (low apical/anterior and apical/mid/base).

Results

Histopathological Findings

MRI/TRUS fusion guided biopsy results were obtained for all 106 patients. There was no available histopathology for 2 MRI lesions which were therefore excluded from analysis. A total of 239 target lesions in 106 patients with corresponding histopathology were evaluated in this study. The median largest size of the target lesion was 9.4mm (mean: 11.0mm, range: 3.0 – 40.0mm). Ninety cancer lesions were identified in 55 of 106 patients. Twenty-one of these patients had multifocal lesions. Eleven patients had 2 sites of malignancy, 7 patients had 3 sites, 2 patients had 4 sites, and 1 patient had 5 sites of malignancy. Of the 90 tumors, 24 tumors were Gleason 6 and 66 tumors were Gleason 7, 8, or 9 (Gleason 7: 33, Gleason 8: 24, Gleason 9: 9) with a mean Gleason score of 7. One patient, accounting for 3 of the 33 Gleason 7 tumors, had Gleason pattern 4+3; the remainder of the Gleason 7 tumors were 3+4 in pattern, thus all Gleason 7 patients are considered as a single group. Biopsy negative MRI targets were often atypia or inflammation at pathology.

Lesion Visibility and Image Quality of calculated High b-value DWI

The b=2000 s/mm^2 DWI depicted a greater number of lesions on both acquired and calculated IVIM DWI than were seen with b=1000 s/mm^2 (acquired or calculated) (Table 2). Higher percentage of bigger lesions (≥10mm, Table 2b) were visible than smaller ones (<10mm, Table 2a). A larger percentage of high-grade tumors were visible on acquired and IVIM-calculated high b-value MRI compared with the DK model (Table 2). Calculated $b1000_{IVIM}$ and $b2000_{IVIM}$ DWI had similar lesion visibility compared to the acquired DWI. However, calculated DWI using the DK model had fewer visible lesions, particularly at b=2000 s/mm^2.

Image quality difference between each pair of the four calculated high b-value DWI ($b1000_{IVIM}$, $b2000_{IVIM}$, $b1000_{DK}$, $b2000_{DK}$) was strongly statistically different ($p<0.001$) for all lesions (Table 3a) and for lesion in PZ and TZ (Table 3c). Image quality difference between each pair was also strongly statistically significant ($p<0.001$) except $b1000_{DK}$ and $b2000_{IVIM}$ ($p=0.091$), b1000IVIM and b2000IVIM ($p=0.0178$) in the low apical and anterior region, and $b1000_{IVIM}$ and $b2000_{IVIM}$ ($p<0.010$), $b1000_{DK}$ and $b2000_{DK}$ ($p<0.010$) in the apical/mid/base region. In all the comparisons, $b1000_{IVIM}$ had best and $b2000_{DK}$ had the worst image quality. Image quality for $b1000_{IVIM}$ vs. acquired b=1000s/mm^2 achieved near equality (97.1%) while the calculated images were of inferior quality for $b2000_{IVIM}$ vs. the acquired b=2000 s/mm^2 DWI (85%). Furthermore, image quality of the calculated high b-value DWI was comparable to the acquired DWI in PZ and apical/mid/base while it was of lower quality in the TZ and low apical & anterior locations (figures 2 and 3).

Discussion

DWI is an important diagnostic tool in the detection of prostate cancer. Although conventional b- value DWI has been reported to improve detection of prostate cancer, high b-value DWI has been shown to be of further value in improving the specificity of DWI for higher grade tumors [19]. However, acquired high b-value DWI is often noisy and may consume additional scan time if regular b-value DWI is already obtained. Our study shows that DWI acquired with regular b- values can be used to produce calculated DWI that simulates acquired high b-value DWI. These images, particularly when generated with the IVIM model, are diagnostically equivalent to acquired high b-value DWI at b=1000s/mm^2 and slightly inferior to acquired high b-value DWI at b=2000s/mm^2. The IVIM model is superior to the DK model in terms of diagnostic quality.

Conventional DWI utilizes b-values between 0–1000 s/mm^2. However, there has been an increasing interest in utilizing higher b-values despite their lower SNR. At higher b-values, only highly restricted water regions are detected, which increases the specificity of DWI for higher grade tumors. Generally acceptable conventional DW images can be obtained at 3.0T with or without an endorectal coil. On the other hand, the lower SNR at b=2000 s/mm^2 often creates non-diagnostic images especially if images are obtained at 1.5T without an endorectal coil. [28]. High b-value DW images result in markedly lower normal tissue signal while maintaining relatively higher signal in water-restricted tissues which increases the specificity of DWI for higher grade tumors however with lower signal to noise ratios (SNR) [29]. Thus, it would be of interest to generate DWI images of similar or better quality at

higher SNR. The Stejskal-Tanner diffusion decay model is affected by perfusion at very low b-values and by non-Gaussian diffusion at very high b-values. Therefore, we chose to calculate high b-value DWI using the IVIM model which accounts for perfusion effects on diffusion and the DK model which accounts for both the effects of perfusion and non-Gaussian diffusion [11–14]. The IVIM and DK models chosen were simplified by fitting the non-zero b-values of the regular b-value DWI to a mono-exponential decay curve [4]. Recently, it has been shown that the noise variance of calculated DWI is lower than that of acquired DWI at the same b-value in phantom experiments [25]. More recently, others have shown the contrast to noise ratio (CNR) for tumors to be comparable for measured and calculated b1400 DWI [29]. In addition, Rosenkrantz et al showed the impact of calculated DWI on prostate MRI [30]. They compared the image quality and tumor detection of acquired and calculated b1500 DWI in 39 patients. There was greater suppression of benign prostate tissue with calculated b1500 DWI than at lower b-value DWI with less distortion and fewer artifacts using calculated vs. acquired b1500 images.

In our 106 patient cohort, which included 239 targeted lesions and 90 tumor positive lesions, we found calculated $b1000_{IVIM}$ and $b2000_{IVIM}$ DWI to detect a similar number of lesions as acquired DWI. While calculated $b1000_{DK}$ had similar lesion detection to acquired DWI, $b2000_{DK}$ was clearly inferior to acquired DWI. We suspect that this is because even though the DK model can accurately model diffusion decay at high b-values, the range of b-values acquired in our regular DWI MRI (b=0–750 s/mm^2) was not adequate to compute the parameters of a DK model [5]. The robustness of DK parameters is of greater importance with higher b-values (e.g. b=2000 s/mm^2 as compared to b=1000 s/mm^2).

Recent studies have suggested that higher b value images are more sensitive for significant prostate cancer. For instance, one study showed the superiority of acquired b=2000s/mm^2 DWI compared to b=1000s/mm^2 DWI [31]. We also found better lesion visibility at b=2000s/mm^2 (72%) compared to b=1000s/mm^2 DWI (55%). At b=1000s/mm^2, both IVIM and acquired DWI have higher lesion visibility for high grade (Gleason 8–9) tumors when compared to low grade (Gleason 6–7) tumors. While at b=2000s/mm^2, similar lesion visibility for both low and high grade tumors suggests the existence of an optimal b-value below b=2000s/mm^2 for separating high and low grade tumors, requiring further investigation.

In order for images to be acceptable for interpretation they must be of sufficient quality for observers to have confidence in them. We directly compared image quality of calculated and acquired DWI at b=1000 and 2000 s/mm^2. The $b1000_{IVIM}$ and $b2000_{IVIM}$ DWI dataset has the maximum number of images that are of comparable image quality to b1000 and b2000 DWI. However, $b2000_{IVIM}$ was clearly inferior in image quality compared to $b1000_{IVIM}$. Therefore, calculated high b-value using IVIM model may only be able to replace acquired DWI up to a certain b-value due to the presence non IVIM diffusion decay at higher b-values.

An improvement in specificity was achieved with high b-value DWI, both calculated and acquired, as fewer non-tumor lesions were visible on high b-value images than with ADC maps alone.. Further, with the exception of $b2000_{DK}$, similar lesion visibility and image

quality were achieved with acquired and calculated high b-value DWI. Both acquired and calculated high b-value imaging increased specificity of tumor detection while maintaining sensitivity for high grade tumors, and therefore high b value DWI has the potential to reduce the number of insignificant cancers detected by biopsy and thereby improve patient care.

There are several limitations of this study. First, the gold standard was MR/TRUS fusion guided biopsy instead of prostatectomy specimens. Increasingly, patients undergoing prostatectomy represent a narrow range of prostate cancer aggressiveness which is not representative of the full gamut of disease. Low grade tumors are often followed with active surveillance whereas higher grade tumors often undergo radiation and hormone ablation therapy and are thus, not represented in series relying on prostatectomy specimens for validation. On the other hand, blind biopsies are justifiably considered to be inaccurate as a gold standard. The advent of MR/TRUS fusion has dramatically improved the accuracy of prostate biopsies and is rapidly becoming the de facto gold standard of validation, however our platform has an accuracy of about 3–4mm for targeting lesions [32]. Another limitation comes from the fact that high b-value DWI calculation is non-linear and it is not straightforward how varying the SNR of individually acquired DW images affects the SNR of calculated high b-value MRI. Therefore, instead of reporting the SNR differences, we have reported the required data acquisition times for DWI datasets. Finally, the two readers in this study interpreted the studies in consensus and therefore, inter-reader variability cannot be determined for acquired vs. calculated DWI.

In conclusion, calculated high b-value DWI based on the IVIM model, is a viable alternative to acquiring high b-value DWI. The DK model proved inferior and is not recommended. Calculated DWI using the IVIM model has equivalent lesion detection and similar image quality to acquired DWI at b1000 but is slightly inferior at b2000. Nonetheless, calculated high b-value DWI produced comparable sensitivities for high-grade cancers which is the most important goal of mpMRI. Thus, calculated high b-value DWI using the IVIM model can replace acquired high b- value DWI at b=1000 s/mm^2 with equal diagnostic value and comparable image quality without additional acquisition time.

References

1. Bonekamp D, Jacobs MA, El-Khouli R, Stoianovici D, Macura KJ. Advancements in MR imaging of the prostate: from diagnosis to interventions. Radiographics : a review publication of the Radiological Society of North America, Inc. 2011; 31(3):677–703. DOI: 10.1148/rg.313105139
2. Thompson J, Lawrentschuk N, Frydenberg M, Thompson L, Stricker P, Usanz. The role of magnetic resonance imaging in the diagnosis and management of prostate cancer. BJU international. 2013; 112(Suppl 2):6–20. DOI: 10.1111/bju.12381
3. Stejskal EO, Tanner JE. Spin Diffusion Measurements: Spin Echoes in the Presence of a Time-Dependent Field Gradient. The Journal of Chemical Physics. 1965; 42(1):288–292. doi:doi:http://dx.doi.org/10.1063/1.1695690.
4. Pang Y, Turkbey B, Bernardo M, Kruecker J, Kadoury S, Merino MJ, Wood BJ, Pinto PA, Choyke PL. Intravoxel incoherent motion MR imaging for prostate cancer: An evaluation of perfusion fraction and diffusion coefficient derived from different b-value combinations. Magnetic resonance in medicine:official journal of the Society of Magnetic Resonance in Medicine/Society of Magnetic Resonance in Medicine. 2012; doi: 10.1002/mrm.24277
5. Jensen JH, Helpern JA. MRI quantification of non-Gaussian water diffusion by kurtosis analysis. NMR in biomedicine. 2010; 23(7):698–710. DOI: 10.1002/nbm.1518 [PubMed: 20632416]

6. Itou Y, Nakanishi K, Narumi Y, Nishizawa Y, Tsukuma H. Clinical utility of apparent diffusion coefficient (ADC) values in patients with prostate cancer: can ADC values contribute to assess the aggressiveness of prostate cancer? Journal of magnetic resonance imaging : JMRI. 2011; 33(1):167–172. DOI: 10.1002/jmri.22317 [PubMed: 21182135]
7. Turkbey B, Shah VP, Pang Y, Bernardo M, Xu S, Kruecker J, Locklin J, Baccala AA Jr, Rastinehad AR, Merino MJ, Shih JH, Wood BJ, Pinto PA, Choyke PL. Is apparent diffusion coefficient associated with clinical risk scores for prostate cancers that are visible on 3-T MR images? Radiology. 2011; 258(2):488–495. DOI: 10.1148/radiol.10100667 [PubMed: 21177390]
8. Hambrock T, Somford DM, Huisman HJ, van Oort IM, Witjes JA, Hulsbergen-van de Kaa CA, Scheenen T, Barentsz JO. Relationship between apparent diffusion coefficients at 3.0-T MR imaging and Gleason grade in peripheral zone prostate cancer. Radiology. 2011; 259(2):453–461. DOI: 10.1148/radiol.11091409 [PubMed: 21502392]
9. Vargas HA, Akin O, Franiel T, Mazaheri Y, Zheng J, Moskowitz C, Udo K, Eastham J, Hricak H. Diffusion-weighted endorectal MR imaging at 3 T for prostate cancer: tumor detection and assessment of aggressiveness. Radiology. 2011; 259(3):775–784. DOI: 10.1148/radiol.11102066 [PubMed: 21436085]
10. Kobus T, Vos PC, Hambrock T, De Rooij M, Hulsbergen-Van de Kaa CA, Barentsz JO, Heerschap A, Scheenen TW. Prostate cancer aggressiveness: in vivo assessment of MR spectroscopy and diffusion-weighted imaging at 3 T. Radiology. 2012; 265(2):457–467. DOI: 10.1148/radiol.12111744 [PubMed: 22843767]
11. Le Bihan D, Breton E, Lallemand D, Aubin ML, Vignaud J, Laval-Jeantet M. Separation of diffusion and perfusion in intravoxel incoherent motion MR imaging. Radiology. 1988; 168(2):497–505. [PubMed: 3393671]
12. DeCarlo LT. On the meaning and use of kurtosis. Psychological Methods. 1997; 2(3):292–307.
13. Jensen JH, Helpern JA, Ramani A, Lu H, Kaczynski K. Diffusional kurtosis imaging: the quantification of non-gaussian water diffusion by means of magnetic resonance imaging. Magnetic resonance in medicine : official journal of the Society of Magnetic Resonance in Medicine / Society of Magnetic Resonance in Medicine. 2005; 53(6):1432–1440. DOI: 10.1002/mrm.20508
14. Rosenkrantz AB, Sigmund EE, Johnson G, Babb JS, Mussi TC, Melamed J, Taneja SS, Lee VS, Jensen JH. Prostate cancer: feasibility and preliminary experience of a diffusional kurtosis model for detection and assessment of aggressiveness of peripheral zone cancer. Radiology. 2012; 264(1):126–135. DOI: 10.1148/radiol.12112290 [PubMed: 22550312]
15. Padhani AR, Liu G, Koh DM, Chenevert TL, Thoeny HC, Takahara T, Dzik-Jurasz A, Ross BD, Van Cauteren M, Collins D, Hammoud DA, Rustin GJ, Taouli B, Choyke PL. Diffusion-weighted magnetic resonance imaging as a cancer biomarker: consensus and recommendations. Neoplasia (New York, NY). 2009; 11(2):102–125.
16. Kitajima K, Kaji Y, Kuroda K, Sugimura K. High b-value diffusion-weighted imaging in normal and malignant peripheral zone tissue of the prostate: effect of signal-to-noise ratio. Magnetic resonance in medical sciences : MRMS : an official journal of Japan Society of Magnetic Resonance in Medicine. 2008; 7(2):93–99.
17. Katahira K, Takahara T, Kwee TC, Oda S, Suzuki Y, Morishita S, Kitani K, Hamada Y, Kitaoka M, Yamashita Y. Ultra-high-b-value diffusion-weighted MR imaging for the detection of prostate cancer: evaluation in 201 cases with histopathological correlation. European radiology. 2011; 21(1):188–196. DOI: 10.1007/s00330-010-1883-7 [PubMed: 20640899]
18. Kim CK, Park BK, Kim B. High-b-value diffusion-weighted imaging at 3 T to detect prostate cancer: comparisons between b values of 1,000 and 2,000 s/mm2. AJR American journal of roentgenology. 2010; 194(1):W33–W37. DOI: 10.2214/ajr.09.3004 [PubMed: 20028888]
19. Metens T, Miranda D, Absil J, Matos C. What is the optimal b value in diffusion-weighted MR imaging to depict prostate cancer at 3T? European radiology. 2012; 22(3):703–709. DOI: 10.1007/s00330-011-2298-9 [PubMed: 21971824]
20. Kitajima K, Takahashi S, Ueno Y, Yoshikawa T, Ohno Y, Obara M, Miyake H, Fujisawa M, Sugimura K. Clinical utility of apparent diffusion coefficient values obtained using high b-value when diagnosing prostate cancer using 3 tesla MRI: comparison between ultra-high b-value (2000 s/mm(2)) and standard high b-value (1000 s/mm(2)). Journal of magnetic resonance imaging : JMRI. 2012; 36(1):198–205. DOI: 10.1002/jmri.23627 [PubMed: 22371381]

21. Koo JH, Kim CK, Choi D, Park BK, Kwon GY, Kim B. Diffusion-weighted magnetic resonance imaging for the evaluation of prostate cancer: optimal B value at 3T. Korean journal of radiology : official journal of the Korean Radiological Society. 2013; 14(1):61–69. DOI: 10.3348/kjr.2013.14.1.61
22. Ohgiya Y, Suyama J, Seino N, Hashizume T, Kawahara M, Sai S, Saiki M, Munechika J, Hirose M, Gokan T. Diagnostic accuracy of ultra-high-b-value 3.0-T diffusion-weighted MR imaging for detection of prostate cancer. Clinical imaging. 2012; 36(5):526–531. DOI: 10.1016/j.clinimag.2011.11.016 [PubMed: 22920357]
23. Ueno Y, Kitajima K, Sugimura K, Kawakami F, Miyake H, Obara M, Takahashi S. Ultra-high b-value diffusion-weighted MRI for the detection of prostate cancer with 3-T MRI. Journal of magnetic resonance imaging : JMRI. 2013; doi: 10.1002/jmri.23953
24. Rosenkrantz AB, Hindman N, Lim RP, Das K, Babb JS, Mussi TC, Taneja SS. Diffusion-weighted imaging of the prostate: Comparison of b1000 and b2000 image sets for index lesion detection. Journal of magnetic resonance imaging : JMRI. 2013; doi: 10.1002/jmri.24016
25. Blackledge MD, Leach MO, Collins DJ, Koh DM. Computed diffusion-weighted MR imaging may improve tumor detection. Radiology. 2011; 261(2):573–581. DOI: 10.1148/radiol.11101919 [PubMed: 21852566]
26. Turkbey B, Xu S, Kruecker J, Locklin J, Pang Y, Bernardo M, Merino MJ, Wood BJ, Choyke PL, Pinto PA. Documenting the location of prostate biopsies with image fusion. BJU international. 2011; 107(1):53–57. DOI: 10.1111/j.1464-410X.2010.09483.x [PubMed: 20590543]
27. Xu S, Kruecker J, Turkbey B, Glossop N, Singh AK, Choyke P, Pinto P, Wood BJ. Real-time MRI-TRUS fusion for guidance of targeted prostate biopsies. Computer aided surgery : official journal of the International Society for Computer Aided Surgery. 2008; 13(5):255–264. DOI: 10.3109/10929080802364645 [PubMed: 18821344]
28. Sciarra A, Barentsz J, Bjartell A, Eastham J, Hricak H, Panebianco V, Witjes JA. Advances in Magnetic Resonance Imaging: How They Are Changing the Management of Prostate Cancer. European urology. 2011; 59(6):962–977. doi:http://dx.doi.org/10.1016/j.eururo.2011.02.034. [PubMed: 21367519]
29. Maas MC, Futterer JJ, Scheenen TW. Quantitative evaluation of computed high B value diffusion-weighted magnetic resonance imaging of the prostate. Investigative radiology. 2013; 48(11):779–786. DOI: 10.1097/RLI.0b013e31829705bb [PubMed: 23907102]
30. Rosenkrantz AB, Chandarana H, Hindman N, Deng FM, Babb JS, Taneja SS, Geppert C. Computed diffusion-weighted imaging of the prostate at 3 T: impact on image quality and tumour detection. European radiology. 2013; doi: 10.1007/s00330-013-2917-8
31. Ueno Y, Takahashi S, Kitajima K, Kimura T, Aoki I, Kawakami F, Miyake H, Ohno Y, Sugimura K. Computed diffusion-weighted imaging using 3-T magnetic resonance imaging for prostate cancer diagnosis. European radiology. 2013; 23(12):3509–3516. DOI: 10.1007/s00330-013-2958-z [PubMed: 23881300]
32. Siddiqui MM, Rais-Bahrami S, Truong H, Stamatakis L, Vourganti S, Nix J, Hoang AN, Walton-Diaz A, Shuch B, Weintraub M, Kruecker J, Amalou H, Turkbey B, Merino MJ, Choyke PL, Wood BJ, Pinto PA. Magnetic Resonance Imaging/Ultrasound-Fusion Biopsy Significantly Upgrades Prostate Cancer Versus Systematic 12-core Transrectal Ultrasound Biopsy. European urology. 2013; doi: 10.1016/j.eururo.2013.05.059
33. Pokorny MR, de Rooij M, Duncan E, Schröder FH, Parkinson R, Barentsz JO, Thompson LC. Prospective Study of Diagnostic Accuracy Comparing Prostate Cancer Detection by Transrectal Ultrasound–Guided Biopsy Versus Magnetic Resonance (MR) Imaging with Subsequent MR-guided Biopsy in Men Without Previous Prostate Biopsies. European urology. 2014; 66(1):22–29. [PubMed: 24666839]

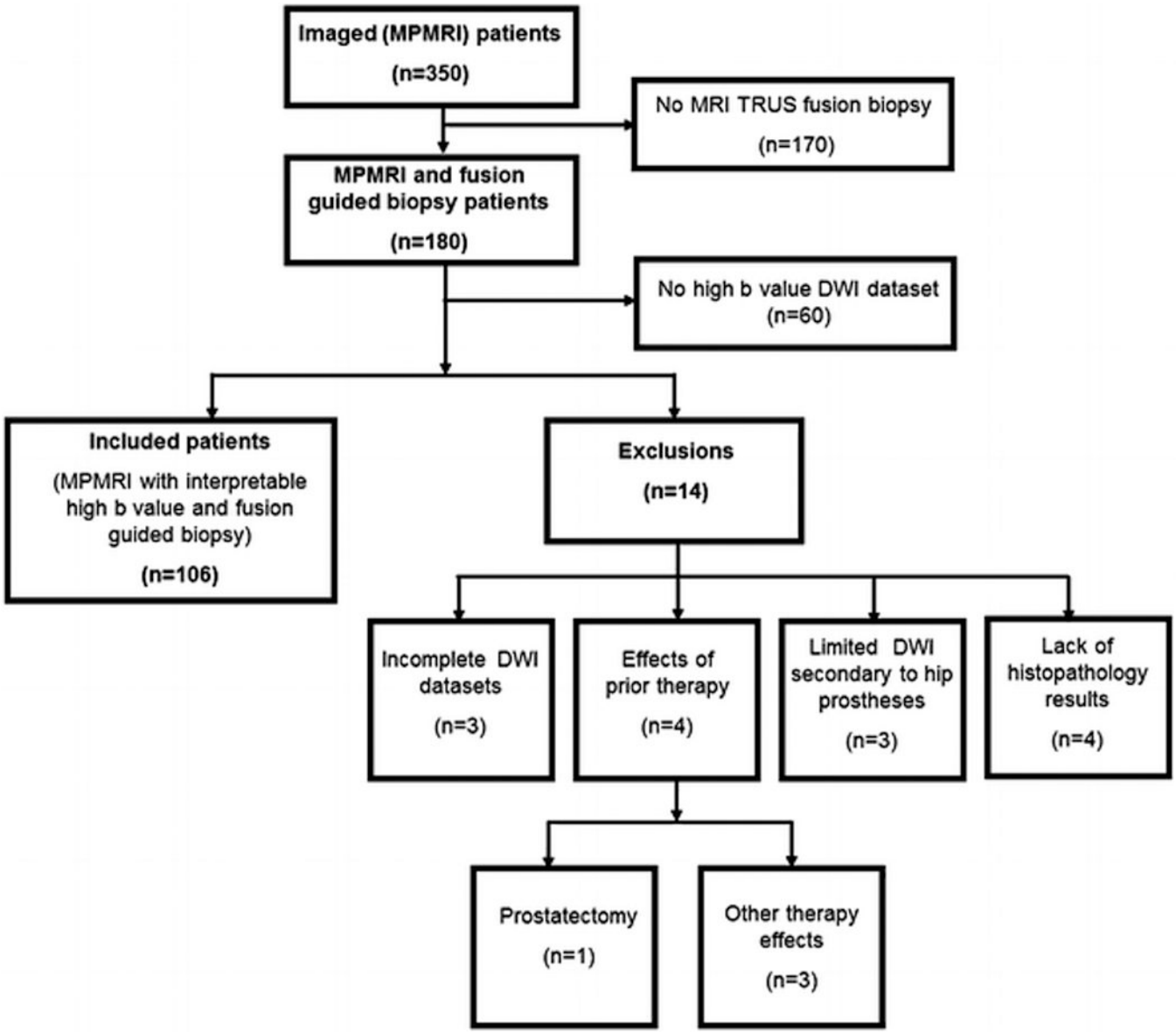

Figure 1.
Study population flow diagram.

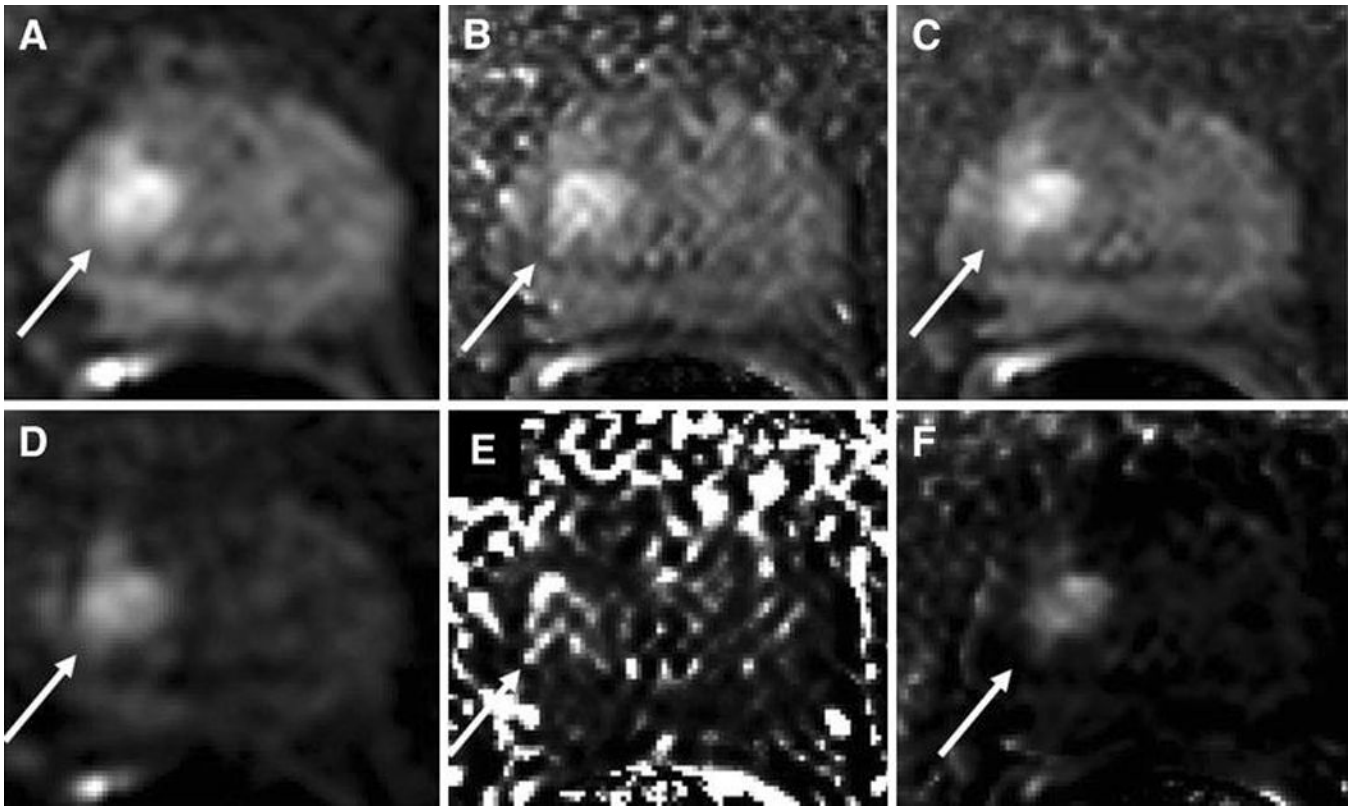

Figure 2.

A 68 year old man with serum PSA of 8.35 ng/mL with apical Gleason 4+3 tumor (10% core involvement). DWI at b=1000s/mm^2 (a) acquired at the scanner and calculated using (b) DK model and (c) IVIM model is shown on top row. Similarly DWI at b=2000s/mm^2 (d) acquired and calculated using (e) DK model and (f) IVIM model is shown on bottom row.

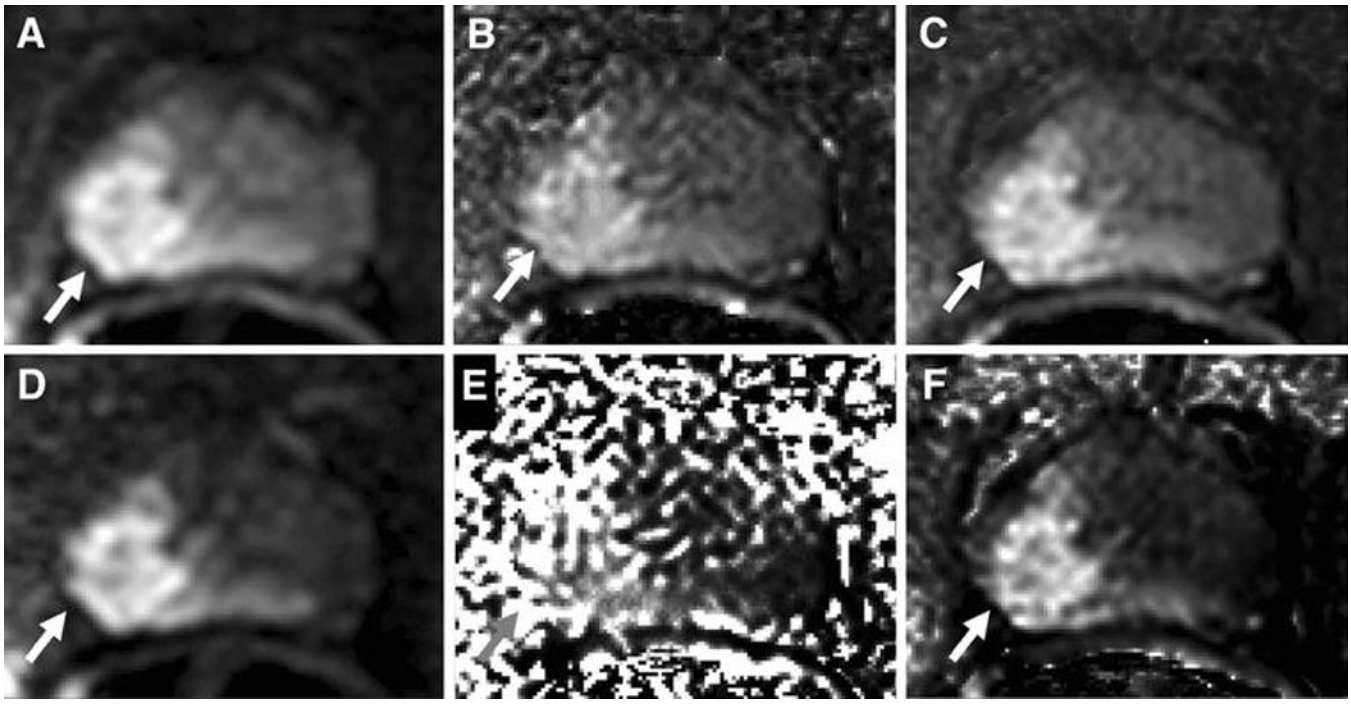

Figure 3.

A 58 year old man with serum PSA of 11.82 ng/mL with right mid-base peripheral zone Gleason 4+5 tumor (70% core involvement). DWI at b=1000s/mm^2 (a) acquired and calculated using (b) DK model and (c) IVIM model is shown on top row. Similarly DWI at b=2000s/mm^2 (d) acquired at the scanner and calculated using (e) DK model and (f) IVIM model is shown on bottom row.

Table 1

MR imaging parameters for regular b-value DWI and high b-value DWI.

	Regular b-value DWI	**High b-value DWI**
Technique	Multi-slice Single-shot SE-EPI	Multi-slice Single-shot SE-EPI
FOV	140mm×140mm	140mm×140mm
Scan Resolution	1.25mm×1.25mm	1.80mm×1.80mm
Scan Matrix	112×108	76×75
Recon Matrix	256×256	256×256
Slices	26	26
Slice Thickness	2.73mm	2.73mm
Slice gap	0.27mm	0.27mm
Orientation	Axial	Axial
Half-scan	0.737	0.732
Water fat shift	minimum (22.482 pixels)	minimum (13.319 pixels)
Bandwidth in EPI frequency direction	1987 Hz	2850 Hz
Fats Suppression	SPAIR	SPAIR
SENSE	2 (RL)	2 (RL)
Gradient Overplus	Yes	Yes
b factor (averages, scan duration)	0 (3, 20sec), 188 (3, 45sec), 375 (3, 45sec), 563 (6, 89sec), 750 (6, 89sec) s/mm^2	0 (1, 14sec), 1000 (5, 105sec), 2000 (5, 105sec) s/mm^2
TR	4873ms	6805ms
TE	52ms	52ms
Scan Time	4min47sec	3min44sec
Diffusion gradient timing DELTA / delta	26.0ms/7.2ms	25.7ms/12.4ms

Table 2

Number of lesions visible on the acquired high b-value DWI and the calculated DWI for all targeted lesions and tumor positive lesions for lesion size less than 10mm (Table 2a) and lesion size greater than 10mm (Table 2b). Percentage of lesions visible among all the corresponding lesions in the cell of the table is noted in parentheses.

	b = 1000s/mm^2			b = 2000s/mm^2		
	Acquired	**DK**	**IVIM**	**Acquired**	**DK**	**IVIM**
All targets (n = 132)	61 (46%)	49 (37%)	61 (46%)	85 (64%)	10 (8%)	90 (68%)
Gleason 6–9 (n = 43)	22 (51%)	17 (40%)	23 (53%)	36 (84%)	7 (16%)	38 (88%)
Gleason 6–7 (n = 30)	14 (47%)	11 (37%)	15 (50%)	27 (90%)	3 (10%)	26 (87%)
Gleason 8–9 (n = 13)	8 (62%)	6 (46%)	8 (62%)	9 (69%)	4 (31%)	12 (92%)

	b = 1000s/mm^2			b = 2000s/mm^2		
	Acquired	**DK**	**IVIM**	**Acquired**	**DK**	**IVIM**
All targets (n = 107)	71 (66%)	65 (61%)	68 (64%)	86 (80%)	30 (28%)	84 (79%)
Gleason 6–9 (n = 47)	35 (74%)	34 (72%)	36 (77%)	42 (89%)	22 (47%)	41 (87%)
Gleason 6–7 (n = 30)	20 (67%)	20 (67%)	21 (70%)	26 (87%)	13 (43%)	25 (83%)
Gleason 8–9 (n = 17)	15 (88%)	14 (82%)	15 (88%)	16 (94%)	9 (53%)	16 (94%)

Table 3

Image quality scores of calculated DWI when compared to acquired DWI for (a) all lesions (b) lesions in low apical & anterior and, apical/mid//base locations (c) lesions in transitional and peripheral zones. Percentage of scored lesions for each calculated DWI is noted in parentheses.

DWI	Score		
	0	**1**	**2**
$b1000_{DK}$	0 (0%)	65 (27%)	174 (73%)
$b1000_{IVIM}$	1 (0.4%)	6 (2.5%)	232 (97.1%)
$b2000_{DK}$	222 (93%)	17 (7%)	0 (0%)
$b2000_{IVIM}$	0 (0%)	35 (15%)	204 (85%)

low apical & anterior

DWI	Score		
	0	**1**	**2**
$b1000_{DK}$	0 (0%)	25 (28.7%)	62 (71.3%)
$b1000_{IVIM}$	1 (1.1%)	3 (3.4%)	83 (95.4%)
$b2000_{DK}$	82 (94.3%)	5 (5.7%)	0 (0%)
$b2000_{IVIM}$	0 (0%)	14 (16.1%)	73 (83.9%)

apical/mid/base

DWI	Score		
	0	1	2
$b1000_{DK}$	0 (0%)	40 (26.3%)	112 (73.7%)
$b1000_{IVIM}$	0 (0%)	3 (2%)	149 (98%)
$b2000_{DK}$	140 (92.1%)	12 (7.9%)	0 (0%)
$b2000_{IVIM}$	0 (0%)	21 (13.8%)	131 (86.2%)

TZ

DWI	Score		
	0	**1**	**2**
$b1000_{DK}$	0 (0%)	28 (31.8%)	60 (68.2%)
$b1000_{IVIM}$	0 (0%)	4 (4.5%)	84 (95.5%)
$b2000_{DK}$	83 (94.3%)	5 (5.7%)	0 (0%)
$b2000_{IVIM}$	0 (0%)	15 (17%)	73 (83%)

PZ

DWI	Score		
	0	1	2
$b1000_{DK}$	0 (0%)	37 (24.5%)	114 (75.5%)
$b1000_{IVIM}$	1 (0.7%)	2 (1.3%)	148 (98%)
$b2000_{DK}$	139 (92.1%)	12 (7.9%)	0 (0%)

	TZ		
DWI	Score		
	0	1	2
$b2000_{IVIM}$	0 (0%)	20 (13.2%)	131 (86.8%)